Cation−Cation "Attraction": When London Dispersion Attraction Wins over Coulomb Repulsion
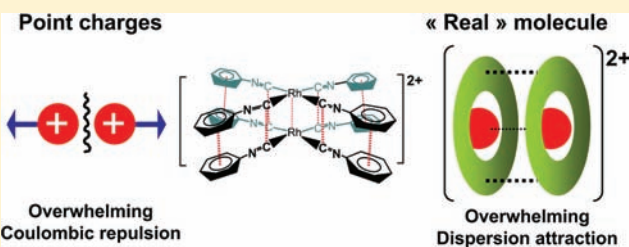
Stefan Grimme*,[†] and Jean-Pierre Djukic*,[‡]

[†]Organisch-Chemisches Institut, Westfälische Wilhelms Universität, Corrensstrasse 40, D-48149 Münster, Germany
[‡]Institut de Chimie, UMR 7177 CNRS, Université de Strasbourg, 4 rue Blaise Pascal, F-67000 Strasbourg, France

S *Supporting Information*

ABSTRACT: London forces are omnipresent in nature and relevant to molecular engineering. Proper tuning of their energetic contribution may stabilize molecular aggregates, which would be otherwise highly unstable by virtue of other overwhelming repulsive terms. The literature contains a number of such noncovalently bonded molecular aggregates, of which the "binding mode" has never been thoroughly settled. Among those are the emblematic cationic complexes of tetrakis(isonitrile)rhodium(I) studied by a number of researchers. The propensity of these complexes to spontaneously produce oligomers has been an "open case" for years. For the dimer $[(PhNC)_4Rh]_2^{2+}$, one of the archetypes of such oligomers, density functional theory methods (DFT-D3) and wave function based spin-component-scaled second-order Møller−Plesset perturbation theory (SCS-MP2) quantum chemical calculations indicate that when the eight isonitrile ligands arrange spatially in an optimal π-stacked fashion, the energy due to dispersion not only overcomes Coulombic repulsion but also the entropy penalty of complex formation. This central role of long-range electron correlation explains such cation−cation attractive interactions. Furthermore, the present findings relativize the role of the metal−metal "d^8−d^8" interactions, which are present on a relatively small scale compared to the effects of the ligands; d^8−d^8 interactions represent about 10−15% of the total dispersion contribution to the binding energy.

INTRODUCTION

It is widely accepted that attractive noncovalent interactions, postulated by van der Waals and formalized by London, are omnipresent in nature.[1] Their role is essential in ensuring the structural cohesion of molecular, nanomolecular,[2] and supramolecular[3] systems and in guiding them into specific structural changes and reaction pathways.[4−10] We recently engaged a wide and systematic assessment of the role of the so-called dispersion (*London* forces) in a large variety of complex chemical situations.[11−25] With dispersion at the forefront of this endeavor,[26−28] methods that can account for long-range correlation interactions are mandatory. From this standpoint, the case of charged molecular aggregates made by association of charged molecules is of utmost importance.[2] Our attention turned to a class of isonitrile complexes of rhodium(I)[29−31] of formula $[(RNC)_4Rh]^+$ which was extensively studied during the past 40 years (Scheme 1). The ability of such complexes to produce oligomers displaying specific chemical and physical properties was highlighted in a large number of reports.[32−39]

The formation of dimers[40,41] and trimers,[42,43] which is always accompanied with major changes in the electronic spectrum,[44−48] sparked conjectures on a specific d^8−d^8 interaction[49−52] that would act somewhat as a driving force of aggregation[53−67] in a way assimilated to the metallophilic[68] attraction between closed shell metal centers. However, not

many investigations[50] have been reported about this somewhat unique process of self-aggregation of cationic molecules. In the present report, evidence is provided as to the central role of London dispersion forces using as a leading example, the case of the $[(PhNC)_4Rh]_2^{2+}$ bis-cation, i.e. $[\mathbf{1}]_2^{2+}$, of which the synthesis, structure, and chemical properties were first reported by Mann, Gordon, and Gray.[36] Note, that our investigation and analyses focus on molecular situations in gas phase or solution. Consideration of the solid state geometries, in which such oligomers are frequently encountered, would require a periodic treatment, which is beyond the scope of the present work.

EXPERIMENTAL SECTION

Diffusion-Ordered NMR Spectroscopy of Solutions of Tetrakis(phenylisonitrile)rhodium(I) Hexafluorophosphate, $[\mathbf{1}]PF_6$. The synthesis of $[\mathbf{1}]PF_6$ was carried out by applying the literature procedure described by Gray et al.[36] The metathesis of the chloride ion for hexafluorophosphate was carried out by adding a saturated aqueous solution of NH_4PF_6 to a saturated brown-colored solution of freshly formed $[\mathbf{1}]Cl$ in absolute ethanol. The resulting suspension was added with a volume of CH_2Cl_2, and the resulting mixture transferred to an extraction funnel and washed thrice with

Scheme 1. Spontaneous Aggregation of Tetrakis-(isonitrile)rhodium Cations

L = R–NC
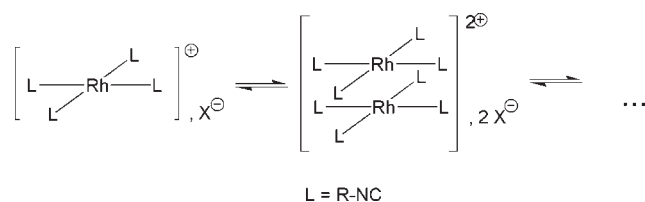
distilled water. The organic phase was dried over $MgSO_4$ and filtered through Celite, and the solvents were removed under reduced pressure to yield a dark green-colored solid. Analytical data collected for $[1]PF_6$ were in full agreement with those published in the literature. Electrospray mass spectrometry in positive mode carried out with a concentrated red-colored solution of $[1]PF_6$ in acetonitrile produced the spectrum of monomer $[1]^+$. A pure sample of $[1]PF_6$ (10 mg, 0.0163 mmol, $c = 32.6$ μM) was dissolved in $d_3 \cdot CH_3CN$ (0.5 mL), and the resulting solution was transferred to a 2.5 mm diameter NMR sample tube for further ^1H DOSY NMR analysis. Diffusion NMR spectroscopy measurements[69] were acquired on a 500 MHz BRUKER Avance spectrometer, outfitted with a BBI 5 mm probe delivering 70 G·cm^{-1}. The sample was prepared in a 2.5 mm tube to restrict the thermal convection, without spinning. The temperature was regulated at 298 and 253 K, and the experiments were performed with a classical limited Eddy current stimulated echo sequence, using a bipolar gradient.[70] DOSY spectra were generated by the DOSY module of NMRNotebook from NMRTEC,[71] using an inverse Laplace transform driven by maximum entropy.[72] At 298 K, sequence parameters were Δ (diffusion time) = 100 ms, δ (gradient length) = 2 × 0.8 ms, τ (gradient recovery delay) = 1 ms, and T_e (LED recovery delay) = 5 ms. At 253 K, sequence parameters were Δ (diffusion time) = 150 ms, δ (gradient length) = 2 × 1.5 ms, τ (gradient recovery delay) = 1 ms, and T_e (LED recovery delay) = 5 ms. Each diffusion measurement required 30 experiments in which gradient strength was increased from 0.5 to 55 G·cm^{-1}. The experiment duration was about 3 h.

Theoretical and Computational Details. Geometry optimization and ground singlet state electronic structure determination were performed using the methods of the density functional theory (DFT). Starting geometries were extracted from the Cambridge Structural Database, wherein compounds $[1]_2^{2+}$, $[2]_2^{2+}$, and $[3]_3^{3+}$ are referenced under the respective "refcodes" RIPICIB, PFICRH, and CEFVUF. The Becke[73]–Perdew[74,75] (BP86) and the Perdew–Burke–Ernzerhof[76] (PBE) GGA functionals as well as the Tao–Perdew–Staroverov–Scuseria (TPSS) metaGGA functional[77] implemented in the Amsterdam Density Functional package[78,79] (abbr. ADF, version 2010.01) and in TURBOMOLE[80] were used and supplemented with dispersion corrections in revision two (D2[81]) or three (D3[82]). The corresponding dispersion-corrected functionals are labeled e.g. BP86-D2, PBE-D2, PBE-D3, and so on. The results of geometry optimizations in the gas phase were hence compared to those geometries computed with functionals devoid of dispersion correction, namely LDA, BP86, PBE, and TPSS. Opposed to a similar functional that is typically termed BP86, the implementation in ADF employs the Vosko–Wilk–Nusair parametrization for the LDA correlation energy part.[83] The PBE functional in ADF2009 and ADF2010 employs the PW92 parametrization of the LDA correlation energy part. In calculations carried out with the ADF package, scalar relativistic effects were treated within the Zeroth Order Regular Approximation (ZORA).[84,85] As a consequence, in all cases ad hoc all-electron TZP (ZORA) and TZ2P (ZORA) basis sets were used. For the former basis set electronic configurations of atoms were described by a triple-ζ Slater-type orbital (STO) basis set for H 1s,

C 2s and 2p, O 2s and 2p, and P 3s and 3p augmented with a 3d single-ζ polarization for O, C, and P atoms. An all-electron STO basis set (TZP) was used for Rh in which core electrons are described with double-ζ functions and valence 4d and 5s orbitals with triple-ζ functions augmented with a 5p single-ζ polarization function.[86] For the TZ2P basis set, the definition included a double-ζ polarization function.[86] Geometry optimizations by energy gradient minimization were carried out in all cases with the D_4, D_{4d}, D_{4h} (for $[1]_2^{2+}$ and $[2]_2^{2+}$), and C_{2h} (for $[3]_3^{3+}$) point group symmetries; the latter are detailed in Table 1. Integration grid accuracy spanned 4.5–6, the energy gradient convergence criterion was set to 10^{-3} au, and tight SCF convergence criteria (10^{-7} au) were used. Interfragment Kohn–Sham orbital interaction analyses were performed with optimized geometries within the ADF package. Wiberg bond indices for ADF-optimized geometries (using all-electron TZP basis sets) were computed with the GENNBO 5.0 extension of ADF.[87] Representations of molecular structures and orbitals were drawn using ADFview v09 and v10. Solvation by acetonitrile ($\varepsilon = 37.5$) was accounted for using the COSMO[88–90] procedure with Klamt's values of van der Waals radii for atoms. Thermodynamic data were computed from the statistical data, namely internal energy and entropy, generated by vibrational frequency calculations. The latter were computed by analytical integration and by two point numerical differentiation for geometries optimized respectively in the gas phase and in acetonitrile (COSMO).[78]

Conformational Computations for $[1]_2^{2+}$. The computations of the different equilibrium conformations of $[1]_2^{2+}$ and the potential energy curve (PEC) by varying the M–M' bond length were carried out with the TURBOMOLE package.[80] In all geometry optimizations by energy gradient minimization D_4 point group symmetry constraints were applied. All optimizations were consistently performed at the COSMO ($\varepsilon = 37.5$) level, and these structures were used in subsequent single-point calculations without these continuum corrections. A large integration grid (m4 in TURBOMOLE notation) and tight SCF convergence criteria have been used. The meta-GGA functional TPSS[78] together with our new DFT-D3 dispersion correction[82] (dubbed TPSS-D3) was used. The corresponding atomic coordinates are provided in the Supporting Information. Single point calculations employing these geometries were performed for comparison also with a wave function based technique. The spin-component-scaled second-order Møller–Plesset perturbation theory (SCS-MP2)[91] has proven fair accuracy also for transition metal complexes and is used here as an alternative to DFT for large systems. If not mentioned otherwise, for all atoms the large def2-TZVP Gaussian basis sets have been used[92] in TPSS and SCS-MP2 treatments. For rhodium, an effective (small) core potential for the 28 inner shell electrons were applied.[92] Basis set convergence has been checked previously[24] for similar bimetallic compounds by comparison with results from the very large and almost complete def2-QZVP basis set.[93] At the TPSS-D3/def2-TZVP association energies (ΔE) are typically about 2–4% larger than at the estimated basis set limit which is small enough for our purposes (and also more accurate than the often applied counterpoise-corrections). The ΔE values are computed as the difference of the total energies of the doubly charged M–M' complex and the optimized singly charged fragments, respectively. For all SCF and perturbation correction calculations, we exploited density fitting approaches (also known as resolution-of-identity, RI) to speed up the calculations. Respective default auxiliary basis sets[94,95] were taken from the program libraries. For SCS-MP2, the frozen core approximation was applied (i.e., only orbitals with orbital energies $> -4E_h$ were included in the correlation treatment). In the calculation of the *potential energy curve* (PEC) using the M–M' distance as a reaction coordinate, severe numerical problems were encountered when optimizations of all other degrees of freedom were attempted. Energies were oscillating and "hysteresis" effects were observed. Because several attempts to cure the problems (switching on/off the COSMO or

Table 1. Geometric Parameters for Oligomers $[1]_2{}^{2+}$, $[2]_2{}^{2+}$, and $[3]_3{}^{3+}$ Computed at Various Levels of Theory

entry	cmpd	theory level	d_m (Å)	d_{ipso} (Å)	α (deg)	ψ (deg)	ω (deg)	conformer
1	$[1]_2{}^{2+}$	LDA/TZP[a]	2.943	3.675	179.8	29.1	17.5	**B**[c]
2	$[1]_2{}^{2+}$	BP86/TZP[a]	3.255	4.702	169.4	30.0	14.0	**B**[c]
3	$[1]_2{}^{2+}$	BP86-D2/TZP[a]	3.059	3.548	181.2	26.9	18.4	**B**[c]
4	$[1]_2{}^{2+}$	BP86-D2/TZ2P[a]	3.052	3.544	181.0	27.4	18.2	**B**[c]
5	$[1]_2{}^{2+}$	BP86-D2/TZ2P[a] (COSMO)	3.055	3.561	181.1	26.5	20.0	**B**[c]
6	$[1]_2{}^{2+}$	PBE/TZP[a]	3.230	5.137	165.6	35.1	27.1	**B**[c]
7	$[1]_2{}^{2+}$	PBE-D2/TZP[a]	3.067	3.602	181.6	28.3	19.4	**B**[c]
8	$[1]_2{}^{2+}$	PBE-D3/TZP[a]	3.185	3.889	171.1	1.9	24.6	**C**[c]
9	$[1]_2{}^{2+}$	TPSS/TZP[a]	3.198	5.143	163.1	31.3	29.0	**B**[c]
10	$[1]_2{}^{2+}$	TPSS-D3/TZP[a]	3.067	4.650	179.6	45.1	1.9	**C−B**[c]
11	$[1]_2{}^{2+}$	TPSS/def2-TZVP[b]	3.183	5.427	167.2	45	93.9	**A**[d]
12	$[1]_2{}^{2+}$	TPSS-D3/def2-TZVP (COSMO)[b]	3.108	3.583	189.0	39.4	71.7	**A**[c]
13	$[1]_2{}^{2+}$	TPSS-D3/def2-TZVP (COSMO)[b]	3.100	3.768	179.8	29.0	13.9	**B**[c]
14	$[1]_2{}^{2+}$	TPSS-D3/def2-TZVP (COSMO)[b]	3.150	3.668	173.5	2.2	17.9	**C**[c]
15	$[1]_2{}^{2+}$	TPSS-D3/def2-TZVP	3.143	3.750	172.3	0	2.8	**C**[j]
16	$[1]_2{}^{2+}$	HF-D3/def2-TZVP	3.656	3.821	177.8	0	0.2	**C**[j]
17	$\{[1]_2(BPh_4)_2\}$	exptl[f]	3.192	3.583	194.3[i]	67.0[i]	38.4	**A**
18	$[2]_2{}^{2+}$	PBE/TZP	3.187	5.080	163.3	59.2	21.2	**B**[c]
19	$[2]_2{}^{2+}$	PBE-D2/TZP	3.162	3.849	181.3	31.4	27.8	**B**[c]
20	$[2]_2{}^{2+}$	TPSS-D3/def2-TZVP[b]	3.129	3.713	179.2	12.8	25.4	**B−C**[c]
21	$\{[2]_2Cl_2\}$	exptl[g]	3.293	3.690[i]	174.8[i]	0.8		**C**
22	$[3]_3{}^{3+}$	PBE/TZP	3.402		159.5	43.4		[e]
23	$[3]_3{}^{3+}$	PBE-D2/TZP	3.053		171.8	46.9		[e]
24	$[3]_3{}^{3+}$	TPSS-D3/def2-TZVP[b]	3.062		171.7	45.3		[e]
25	$\{[3]_3Cl_3\}$	exptl[h]	3.087		169.3	45.9		

[a] STOs, all-electron basis sets, ZORA relativistic treatment. [b] GTOs, relativistic 28 electron ECP for Rh. [c] D_4 symmetry. [d] D_{4d} symmetry. [e] C_{2h} symmetry. [f] From reference 96. [g] From reference 41. [h] From reference 42. [i] Averaged value. [j] D_{4h}.

dispersion corrections, increasing grid size, and decreasing SCF convergence thresholds) failed, we finally decided to construct the PEC from optimized monomer coordinates without further relaxation (i.e., with fully staggered D_{4h} dimer structures, see below). While this should yield qualitatively reliable curves, they miss relaxation effects (i.e., the monomers are kept planar instead of allowing to tilt the PhNC units) at short M−M′ distances where the energies are too high by about 10−20% of dissociation energy D_e.

■ RESULTS AND DISCUSSION

Spectroscopic Evidence of the Presence of $[1]_2{}^{2+}$ in Solution by ^{1}H DOSY NMR. The oligomerization of cationic [tetrakis(alkyl-or aryl-isonitrile)]Rh(I) complexes occurs readily in solvents of high dielectric constant (water, acetonitrile). With solvents of medium to low dielectric constant (dichloromethane, tetrahydrofurane), the anion−cation pair remains supposedly tight enough to prevent the formation of any oligomer. This property was thoroughly investigated by Gray et al. with millimolar concentrations of various salts of cation $[1]^+$ in acetonitrile.[36,96]

The authors established the constants of association K_1 (35 M^{-1}) and K_2 (10 M^{-1}) (Scheme 2) by UV−visible spectroscopic means with solutions of $[1]PF_6$ dissolved in acetonitrile at room temperature at a constant and large ionic strength.[36,96] The related values of reaction free enthalpies ΔG_1° and ΔG_2° (−2.1 and −1.3 kcal/mol respectively) clearly characterize spontaneous transformations. Additional confirmation of the existence of $[1]_2{}^{2+}$ in solution was acquired in this study using diffusion-ordered ^{1}H NMR spectroscopy. The hydrodynamic dimensions of the dissolved species in d_3·MeCN were obtained from the Stoke−Einstein equation applied to solutes in liquid solvents by assuming oblate ellipsoid shapes for both $[1]^+$ and $[1]_2{}^{2+}$.

The ^{1}H DOSY spectrum measured for a solution of $[1]^+$, PF$_6^-$ in d_3·CH$_3$CN (c = 32 μM, 298 K) displayed a continuous trace presenting two maxima respectively at 1250 and 880 μm^2·s^{-1}. The highest and lowest values of diffusion coefficients were consistently assigned to cation $[1]^+$ and bis-cation $[1]_2{}^{2+}$. The molecular dimensions inferred from DOSY ^{1}H NMR data proved to be in good agreement with the dimensions of the van der Waals molecular volumes of $[1]^+$ and $[1]_2{}^{2+}$ computed with models of the experimental structure (vide infra).

Structures. Rh(I),Rh(I) dimers of the type studied here demonstrate what Mann, Gray et al. would call "deformational isomerism", i.e., situations whereby similar or identical assemblies would display, due to shallow energy minima, significantly different geometrical and structural features.[42,43,97] Therefore, a conformational search for low-energy gas-phase structures of $[1]_2{}^{2+}$ was performed based on the original X-ray data of $\{[1]_2,(BPh_4)_2\}$. In the crystal,[96] the compound has no symmetry and is distorted by counterions that are close to two of the phenyl rings. The experimental structure is closest to the computed conformer **A** (D_4 symmetry, see Figure 2a). It is characterized by a partly staggered arrangement of the phenyl rings that are tilted by about 67.7° relative to the M(NC)$_4$ plane formed by one monomer (Table 1, entry 12); the latter being computed as

Scheme 2
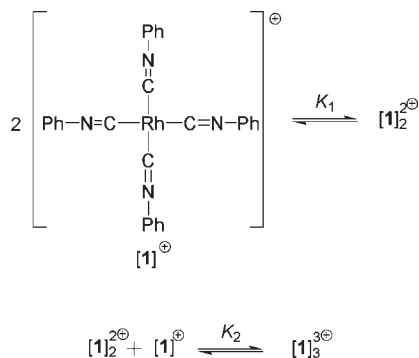
planar (D_{4h}) in its equilibrium structure. The dihedral eclipsing angle ψ (Table 1, entry 13) is about 39.5°. The computed $M-M'$ distance, i.e. d_m, in **A** is ca. 3.11 Å, which is in reasonable agreement with the experimental value of 3.19 Å.

The conformational energy hyper-surface for the dimer and the corresponding interconversions are rather complicated and full exploration of this is beyond the scope of our work. In addition to **A**, two other stable minima **B** and **C** were found (Figure 2a, Table 1, entries 13 and 14). They differ from conformation **A** by much less tilting of the phenyl rings (about 15° for **B** and **C**), and an almost fully eclipsed conformation of the two units (conformer **C**). Although no other crystallographic polymorph of $\{[1]_2(BPh_4)_2\}$ is known, the structure of the fluorine-containing compound $\{[2]_2Cl_2\}$ (Figure 3, Table 1, entry 21),[41] wherein the two mononuclear moieties are almost perfectly *syn*-eclipsed gives reasonable credit to conformer **C**.

We furthermore considered a fully eclipsed structure with D_{4h} symmetry (i.e., $\psi = 0$, $\omega = 0$, Table 1, entry 15) only about 5 kcal/mol higher in energy than **A** (vide infra), which was used as a model structure for the analysis of the interaction (see next section). We also note that conformer **A** is structurally relatively close to a fully staggered D_{4d} conformer (i.e., $\psi = 45$, $\omega = 90$), which is only 1.1 kcal/mol higher in energy. Both structures **A** (D_4) and **A** (D_{4d}) maximize their absolute dispersion energy compared to **B** and **C** by almost doubling the number of phenyl stacking contacts.

It is worthy to note that most dispersion-devoid DFT functionals of GGA type "produce" minimum geometries **B** (Table 1). Table 1 displays the main geometrical features of ground state singlet minimum energy structures obtained at various levels of theory and symmetries. Listed are the values (Figure 2b) of intermetallic distance d_m, interannular distance d_{ipso}, angle α defined by the $C_{ipso}-Rh-C_{ipso}$ angle, the minimal torsion angle ψ around the Rh–Rh axis between two mononuclear moieties, and ω the minimal torsion angle of the phenyl groups with respect to the plane defined by the four carbon atoms bonded to Rh. Table 1 shows that dispersion correction-devoid functionals have a more "repulsive" inclination; they produce geometries with the longest d_m and d_{ipso} distances and smaller α angles (Table 1, entries 2, 6, 9, 11, 18, 22) (vide infra). In general, choice of the density functional (BP86, PBE, TPSS) or other details of the calculation (STO or GTO basis functions, solvation effects, D2 or D3 version of the dispersion correction) has a much smaller effect than "switching" the dispersion "on" or "off". For the important parameter d_m, we find dispersion-induced bond-shortening effects of 0.15–0.2 Å. In the case of oligomer $[3]_3^{3+}$, the effect is even

stronger, with a difference amounting 0.34 Å (Figure 3, Table 1, entries 22−23). A notable exception regarding the different density functionals is the LDA geometry (Table 1, entry 1), which resembles more that of the dispersion-corrected (meta)GGA functionals. LDA simulates dispersion effects at small inter-fragment distances by systematic exchange overbinding ("good results for the wrong reason"). However, LDA typically does not yield consistent results for noncovalent interactions and in our case this inconsistency is evident from the significant underestimation of d_m in spite of the "good" description of the d_{ipso} values and the torsion angles.

Electronic Structure of Dimer $[1]_2^{2+}$ and Bonding. Investigations of the electronic structure of dimer $[1]_2^{2+}$ at the orbital level were carried out using the (ZORA) BP86-D2/TZ2P approach with a singlet ground state geometry optimized in the gas phase. Separate NBO (Natural Bond Orbitals) and NPA (Natural Population Analysis) analyses were carried out with a BP86-D2/TZP geometry. No COSMO corrections are applied. Again, choice of the technical details used in this analysis does not significantly affect our conclusions. The electronic structure was investigated by performing a fragment interaction analysis, which provided the decomposition of the contributions of relevant Kohn−Sham orbitals of $[1]^+$ in the molecular orbital diagram of $[1]_2^{2+}$ (Figure 4a). The in-phase and out-of-phase interactions of the HOMO (metal centered with 79% and 18% contribution of $4d_{z^2}$ and 5s Rh orbital character) of the monomer (orbital 130) is supplemented with a moderate contribution of the π-type LUMO orbital of the monomer (orbital 131, 10% Rh p_z, 13% C p_z, and 17% N p_z character). The latter contributes up to 4% to antibonding orbital 260 and to 1% to bonding orbital 253. Orbitals 253 and 260 in the dimer are stabilized by ca. 3 and 1 eV relative to the "parent" orbital 130 in the monomer. The NPA charges at Rh and at the immediate C and N atoms in the dimer are respectively: $q_{Rh}= -0.001_5$, $q_C = +0.299_6$, $q_N = -0.328_0$; the overall natural charge borne by the phenyl moiety is $+0.221_2$.

The general downshift of orbital energies in the complex is attributed to the doubled positive charge in the complex and has no further physical meaning. This orbital interaction diagram points a typical 4 electron−2 orbital interaction, i.e., a nonbonding situation that is corroborated by the low value of the Wiberg bond index of 0.018 computed from the Natural Atomic Orbital basis for the Rh−Rh segment.

Further scrutiny of the electrostatic potential (ESP) map (cf. Supporting Information) demonstrated the absence of build up of electronic charge density at the two metal centers and a rather large delocalization of the positive charges over each mononuclear fragment. Using the delocalized Mulliken partial charges computed from an equilibrium TPSS-D3 structure and Kohn−Sham-wave function, the electrostatic (ES) interaction of the fragments was estimated to a large value of 43 kcal/mol, which is much smaller than the repulsive interaction of 110 kcal/mol for two point charges centered on the metals. The "true" ES interaction energy computed from the electron densities (TPSS/def2-TZVP) amounts 17 kcal/mol, i.e. a value smaller than that inferred from the point-charge estimate by virtue of charge-density penetration effects.

Nonetheless, in geometries arising from the use of "dispersion correction-devoid" functionals (Table 1), a marked distortion of the square planar environment is noticed ($\alpha < 180°$). This distortion has two origins.

The first is the strong Pauli/electrostatic repulsion between the ligands that carry most of the Coulombic repulsive energy term, the Rh atoms being nearly neutral.
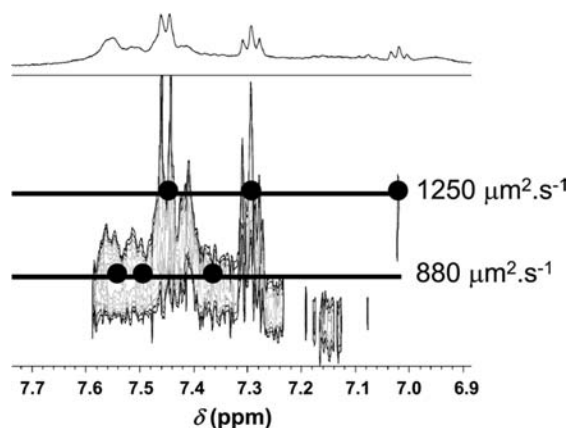
Figure 1. ¹H DOSY NMR trace of a 32.6 μM solution of [1]PF₆ in $d_3 \cdot$MeCN at 298 K. The highest and lowest values of diffusion coefficients correspond respectively to monomeric cation [1]⁺ and bis-cation [1]₂²⁺. Assuming oblate ellipsoid shapes for the analytes, [1]⁺ presents major and minor diameters of 19.0 and 4.5 Å, and [1]₂²⁺ presents major and minor diameters of 19.0 and 7.0 Å.
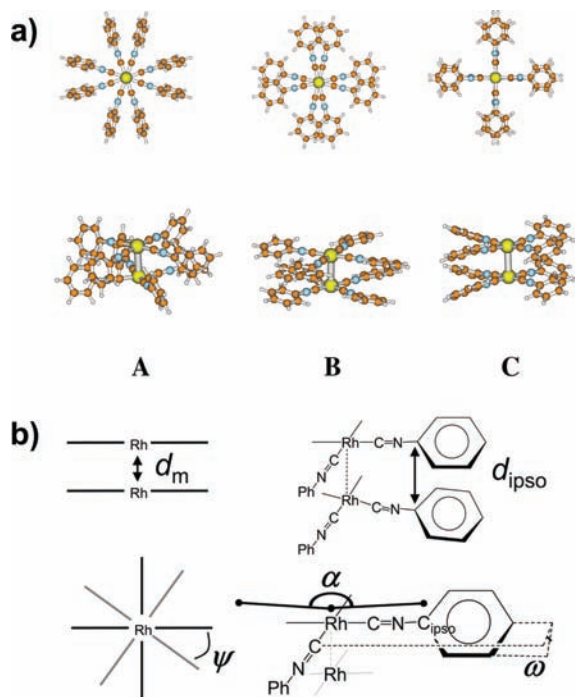

Figure 2. (a) Optimized singlet ground state structures (COSMO TPSS-D3/def2-TZVP) of the three different conformers **A**−**C** of [1]₂²⁺. In **B** and **C**, the Rh−Rh distances, i.e d_m, are merely affected by the conformational changes (d_m= 3.10 and 3.15 Å for **B** and **C**, respectively, Table 1, entries 13 and 14). (b) Description of the geometric parameters listed in Table 1.

The second is a consequence of the neutral character of the Rh atoms, which suggests that attractive short-range correlation-based d⁸−d⁸ interactions may exist. This explains why dispersion correction-devoid functionals produce "associative assemblies" even though these are thermodynamically disfavored (cf. next section).

This is illustrated in Figure 4b, in which the optimized D_{4h} structures at the TPSS-D3 (Table 1, entry 15) and Hartree−
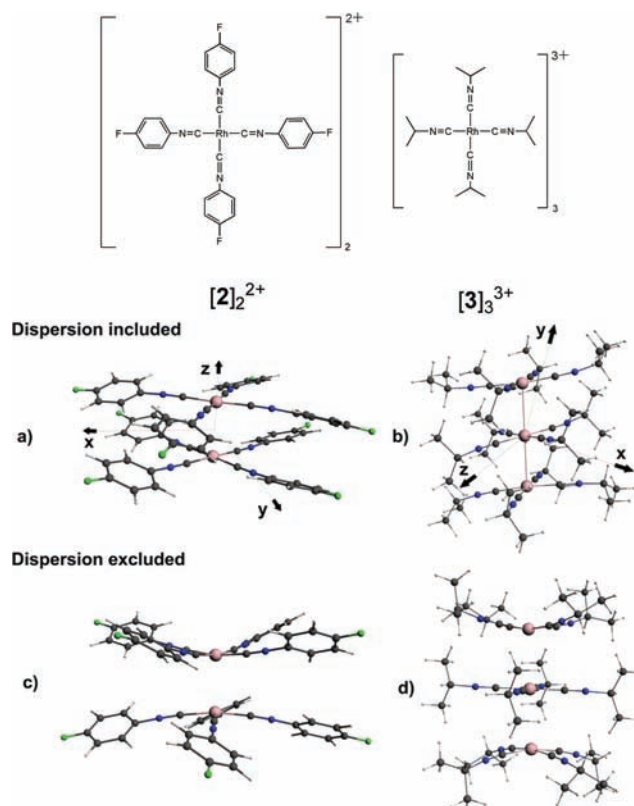

Figure 3. Singlet ground state geometries of [2]₂²⁺ and [3]₃³⁺ computed with and without dispersion corrrection: (a) [2]₂²⁺, PBE-D2 (ZORA)/all-electron TZP; (b) [3]₃³⁺, PBE-D2 (ZORA)/all-electron TZP; (c) [2]₂²⁺, PBE (ZORA)/all-electron TZP; (d) [3]₃³⁺, PBE (ZORA)/all-electron TZP.

Fock (HF)-D3 (Table 1, entry 16) level are compared. While the interannular distances are very similar (3.75−3.83 Å) in both methods due to the similar representation of long-range dispersion by the D3-scheme, d_m is strongly affected by the suppression of the effects of short-range electron correlation in HF-D3: by comparison of the TPSS-D3 and HF-D3 d_m values, an estimate of 0.5 Å for this Rh−Rh electron correlation effect is obtained. This analysis points to a significant contribution of short-range mutual attraction of the two metals by electron correlation, in addition to the long-range dispersion interligand attraction (cf. next section).

Association Energy, Free Enthalpy, and Potential Energy Curves. The formation energies for [1]₂²⁺ from two monocations are given in Table 2 together with contributions from the dispersion and COSMO corrections. In agreement with the experimental observation, at the full TPSS-D3 (COSMO) level, conformer **A** is found to be the most stable. Conformers **B** and **C** are 0.9 and 3.0 kcal/mol, respectively, higher in energy. Note that this energetic ordering **A** < **B** < **C** changes completely to **A** > **B** > **C** when either the dispersion correction (second row in Table 2) or COSMO is switched off. Hence, these corrections are essential already for a qualitatively correct description of this system. The association energies are negative (bound dimer state) only at the TPSS-D3/COSMO level. The dispersion correction to binding is very large (about −43 kcal/mol for **A**). Thus, even when the electrostatic repulsion is screened in solution, the molecular state becomes unbound when dispersion is neglected (TPSS (COSMO) in Table 2).
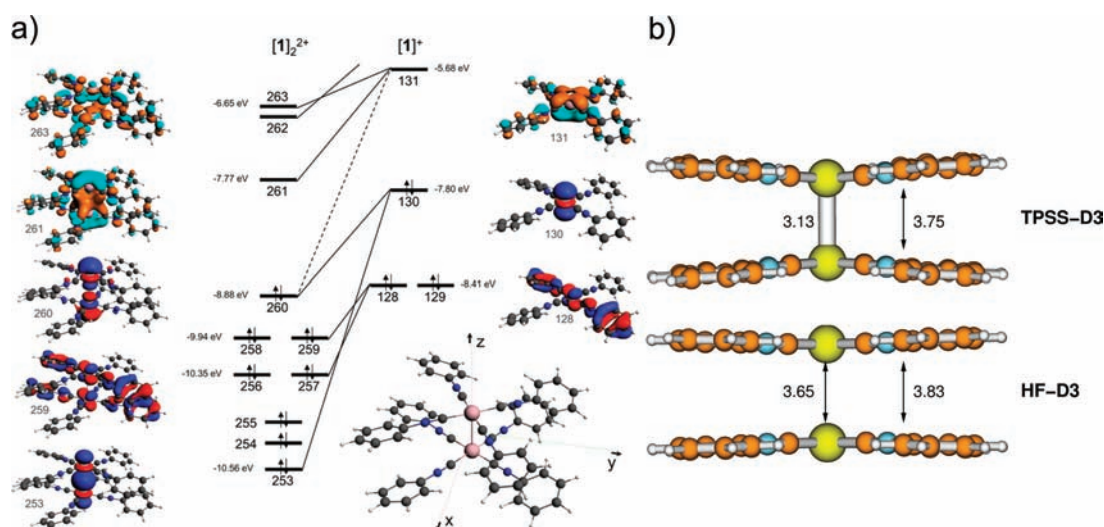
Figure 4. (a) Orbital interaction diagram for dimer $[1]_2^{2+}$ (nonrelaxed fragments). The phases of occupied orbitals and virtual orbitals are colored arbitrarily in red−blue and cyan−orange, respectively. The Wiberg bond index for the Rh−Rh interaction amounts to 0.01_8 for the ground-state geometry computed in the gas phase at the (ZORA) BP86-D2/all-electron (STO) TZ2P level of theory. (b) Effect of the suppression of short-range electron correlation on the distance d_m and d_{ipso} in the gas-phase D_{4h} conformer of $[1]_2^{2+}$ computed at the TPSS-D3/def2-TZVP and HF-D3/def2-TZVP levels. No COSMO corrections are applied.

Table 2. Formation (Association) Energies and Free Enthalpies (in kilocalories per mole) for Three Conformers A−C of $[1]_2^{2+a}$

conformer	A	B	C
ΔE (TPSS-D3/COSMO)	−26.2	−25.3	−23.2
ΔE (TPSS/COSMO)	+16.7	+11.2	+10.5
ΔE (TPSS)	+48	+42.9	+41.8
$\Delta G°_{298}$(TPSS-D3/COSMO)	−7.3	−6.4	−4.3
$\Delta G°_{298}$(TPSS/COSMO)	+35.6	+30.1	+29.4
$\Delta G°_{298}$(TPSS)	+66.9	+61.8	+60.7
ΔE (BP86-D2/COSMO)	-	−25.3	-
ΔE (BP86-D2)	-	+7.4	-
$\Delta G°_{298}$ (BP86-D2/COSMO)^a	-	−12.1	-
$\Delta G°_{298}$ (BP86-D2)^a	-	+26.3	-
$\Delta G°_{298}$ (Expl)^b	-	−2.1	-

^{a} zero-point-vibrational energy, thermal and entropic corrections have been obtained at the ZORA-BP86-D2/TZ2P level of theory; statistical thermodynamic data were computed from pertinent vibrational data. The latter were computed for gas-phase and COSMO optimized geometries of $[1]^+$ and $[1]^{2+}$ (alike of conformer **B**) by analytical integration and by numerical difference respectively. ^{b} computed from ref ^{96} ^{a} Values without solvent (COSMO) and London dispersion contributions are given separately. Negative values indicate a bound molecular system. Values of $\Delta G°_{298}$ are provided for the following reaction: $2[1]^+ \rightarrow [1]_2^{2+}$. For structures of conformers **A−C**, see Figure 1.

This is one of the most important results of our study: when many bulky groups come spatially close and can arrange in an almost optimal fashion (stacking of phenyl rings here), their combined attractive dispersion interactions can overcompensate even the strong Coulomb repulsion between two formal charges. However, this only holds for the condensed phase as their unscreened interaction is slightly larger than the dispersion energy by about 5 kcal/mol for **A**.

When zero-point-vibrational energy, thermal, and entropic corrections are made, the computed free energy of association can be directly compared to the experimental value as derived from measurements of the association equilibrium constants. Although our theoretical result of −7.3 kcal/mol (TPSS-D3-COSMO/def2-TZVP+BP86-D2 vibrational corrections) contains contributions with relatively large estimated errors (mainly from the solvation treatment), it compares reasonably well with the experimental value of −2.1 kcal/mol. Totally inconsistent results would have been obtained for $\Delta G°_{298}$ if the dispersion correction was not included.

The plots of potential energy curves (PEC) in the rigid monomer approximation for the D_{4h} symmetric model structure strongly underline these conclusions (Figure 5a). Without any correction (plain DFT), the PEC is entirely repulsive and shows on the expected $1/R$ asymptotic behavior from the Coulomb potential from about $d_m = 5$ Å. This is effectively screened out in CH_3CN solution as can be seen from the (dispersion uncorrected) DFT (COSMO) curve, which shows already at a distance of about 6 Å no significant interaction anymore. Note that no minimum is observed when dispersion is neglected. This totally repulsive behavior seems to contradict the results of the geometry optimizations that yield bound equilibrium structures for the dimer even without dispersion corrections. The explanation for this is rooted in the PhNC moieties that "lock" the structures by tilting and twisting. These "secondary" conformational changes eventually lead to barriers in the dissociation channel that are not contained in our simplified PEC. Also the remaining attractive Rh−Rh correlations mentioned above can hold the fragments together even when no dispersion correction is applied and the phenyl rings are allowed to bend upward ($\alpha < 180°$).

The dispersion corrected curves (labeled -D3) are qualitatively different. Even in the "gas phase", the dimer now becomes bound although the minimum is still above the asymptote because $1/R$ is much more long-ranged than dispersion ($1/R^6$ decay behavior). The PEC has the right shape and a reasonable
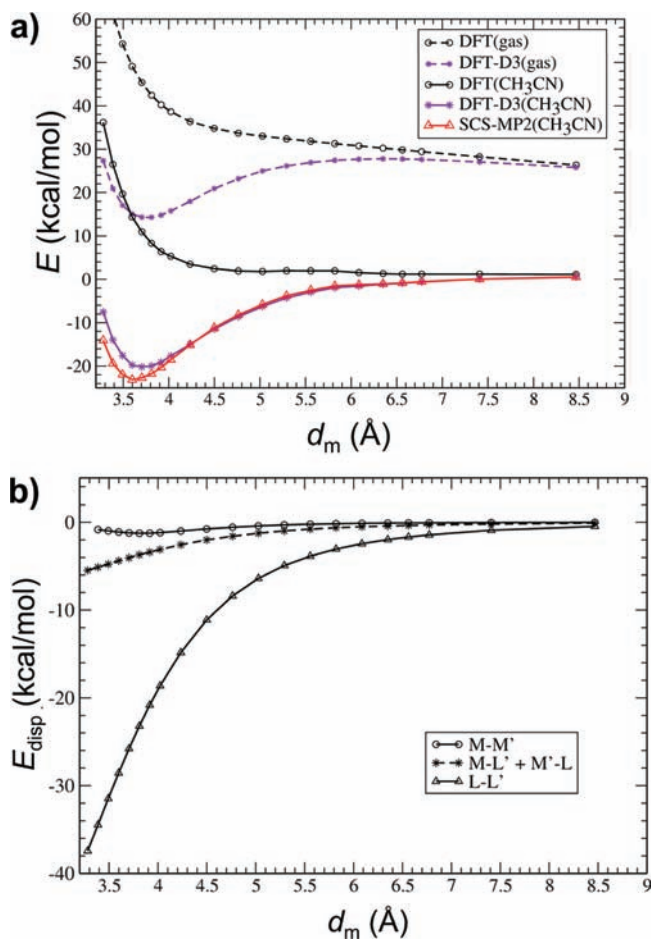
Figure 5. (a) Potential energy curves for $[1]_2^{2+}$ in the gas phase and acetonitrile solution (COSMO) with and without London dispersion corrections ("-D3"). Rigid monomer structures were used in the D_{4h} symmetric dimer model that closely resembles conformer **C**. For comparison, wave function based SCS-MP2/def2-TZVP results are also shown. Small deviations are found only near the equilibrium where SCS-MP2 behaves as "more binding" by about 2 kcal/mol. This can be attributed to a larger basis set superposition error in the SCS-MP2 treatment compared to DFT for which it is expected to be less than 5% of the interaction energy. (b) Dispersion contributions (TPSS-D3) of the metal atoms and ligand fragments to the dissociation of $[1]_2^{2+}$.

energetic position only when dispersion and electrostatic screening are used together. The validity of the DFT-D3 treatment was checked by comparison to a SCS-MP2 wave function-based calculation that intrinsically accounts for dispersion energy. In spite of the large total charge of the complex that may affect the accuracy of DFT-D3, the SCS-MP2 and TPSS-D3 data match very closely in particular in the medium distance range where dispersion is still important.

In DFT-D3, the dispersion energy can easily be partitioned into contributions of molecular fragments.[98,99] The dispersion energy between the two metals ($M-M'$), between each metal atom and the other ligand ($M-L'$ and $M'-L$), and between the ligands ($L-L'$) at the TPSS-D3 level are plotted in Figure 5b. The $L-L'$ term is by far dominating as expected for such large moieties comprising of eight phenyl rings. Note the very large absolute dispersion energy of >40 kcal/mol near equilibrium distances. The minimum in the $M-M'$ curve results from the necessary damping function in DFT-D3 because the metal atoms
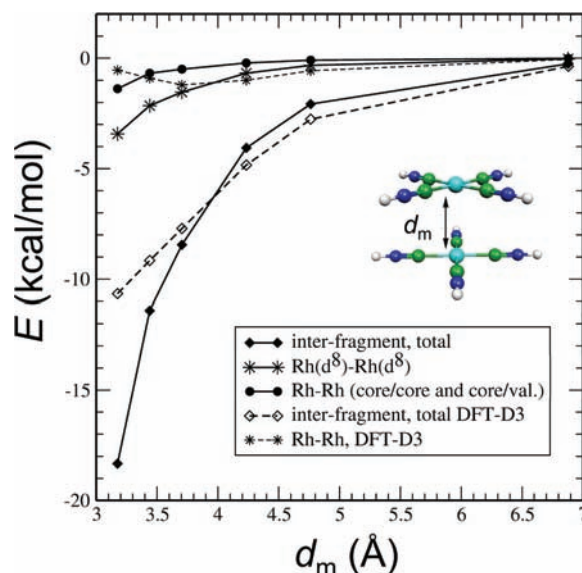

Figure 6. Comparison of interfragment correlation energies [SCS-LMP2/def2-TZVP ($-f$ on C,N; $+f$ on Rh), no COSMO correction] and dispersion contributions (TPSS-D3) of the metal atoms and ligand moieties (e.g., $-$CNH) to the dissociation energy of a model without phenyl rings for $[1]_2^{2+}$ (see inset).

are rather large (the cutoff distance for Rh$-$Rh is about 3.9 Å in TPSS-D3).

In conclusion, we find that long-range dispersion effects between the metals are unimportant. The attractive electron correlations between the filled d^8-shells are certainly present but should better be termed "medium-range" correlation effects.[100] In DFT-D, they are described by the density-dependent part of the underlying exchange-correlation functional and therefore do not appear in this analysis. However, because the question about the importance of d^8–d^8 correlation is important for a general understanding, further analysis was performed using localized orbitals (SCS-LMP2). The latter method has already proven its efficiency to evaluate the intermetallic correlation contribution for bonding.[24] The results using a model system with D_{4d} symmetry and in which phenyl groups were replaced by hydrogen atoms are shown in Figure 6.

One can notice the very good match between the corresponding wave function based and DFT-D3 data also when partitioned, which provides further evidence for the physically sound description of dispersion in the atom-pairwise approach. According to the SCS-LMP2 data, d^8–d^8 valence correlation contributes by about -3.5 kcal/mol to binding near the equilibrium distance (-4.4 kcal/mol for LMP2). Core (i.e., 4s4p) and core$-$valence correlation between the metals add another -1.3 kcal/mol to binding. These values are significant and explain why some intermetallic attraction is even found in dispersion-uncorrected DFT optimized geometries; the values are however lower than for the corresponding 5d^{10}–5d^{10} contribution for Au(I)$-$Au(I) systems which amounts -6.7 kcal/mol at the MP2 level.[101] The corresponding value for silver (4d^{10}–4d^{10}) of about -4 kcal/mol compares reasonably well with our estimate for Rh$-$Rh. Note worthy are also the much smaller total interfragment dispersion energies when the phenyl rings are replaced by hydrogen atoms (cf. Figure 6).

The overestimation of the complex stability compared to experiment by TPSS-D3 could result from an exaggeration of

2625

dx.doi.org/10.1021/ic102489k |*Inorg. Chem.* 2011, 50, 2619–2628

the C_6 coefficients for positively charged systems by DFT-D3, which does not account for changes in the electron number. However, we consider this as being unlikely because (1) the oxidation of the corresponding neutral system $[L_4Rh]^0$, for which DFT-D3 would be expected to be physically "right", causes only a tiny change of the total number of electrons and (2) good agreement between SCS-MP2 and TPSS-D3 computations is found for the model system.

CONCLUSION

In summary, the Coulomb repulsion between two positive point charges at a separation of 3.1 Å is about 110 kcal/mol. If the charges are delocalized over medium-sized molecular fragments ($[1]^+$ in our case), the repulsion is obviously smaller but still on the order of about 40 kcal/mol in the equilibrium structure. There are only two ways for this very unfavorable interaction to be overcome so that a stable doubly charged complex can be formed: first by making a strong covalent bond which at least in principle easily can pay off the Coulombic repulsion. This is clearly not the case in our example. The only other possibility is the action of the ubiquitous, entirely attractive London dispersion forces. When the eight PhNC moieties arrange spatially in an optimal π-stacked fashion, the energy gain is on the order of the Coulomb repulsion. In the case treated here, dispersion is overwhelming, it eventually drives the formation of a stable complex in solution. For $[1]_2^{2+}$, the computed total fragment interaction energies are very large on an absolute scale (about -25 kcal/mol), which leads to computed free energies of association of -7 kcal/mol in fair agreement with available experimental data. This investigation shows that dispersion can also overcome the entropy penalty of complex formation. The present findings relativize the role of the metal−metal d^8−d^8 interactions, which are present on a relatively small scale (about $10-15\%$ of the total dispersion contribution to the binding energy) compared to the effects of the ligands. A further outcome of our study is the sensitivity of the ligand's conformations to the presence of dispersion corrections in standard DFT treatments: without these, computation leads to qualitatively wrong structures, which might be a decisive issue also in other computational studies of metallo-organic systems.

ASSOCIATED CONTENT

S **Supporting Information.** (1) Extensive listing of Cartesian coordinates of the main structures, (2) energies, (3) vibrational frequencies and associated statistical thermodynamic data. This material is available free of charge via the Internet at http://pubs.acs.org.

AUTHOR INFORMATION

Corresponding Author

*E-mail: grimmes@uni-muenster.de. Phone: +49 251 83-33241 (S.G.). E-mail: djukic@unistra.fr. Phone: +33 368851523 (J.-P.D.).

ACKNOWLEDGMENT

REFERENCES

(1) (a) London, F. *Z. Phys.* **1930**, *63*, 245–279.(b) Stone, A. J. *The Theory of Intermolecular Forces*; Oxford University Press: Oxford, 1997. (c) Hobza, P.; Müller-Dethlefs, K. *Non-covalent interactions. Theory and experiment*; The Royal Society of Chemistry: Cambridge, 2010.

(2) Rance, G. A.; Marsh, D. H.; Bourne, S. J.; Reade, T. J.; Khlobystov, A. N. *ACS Nano* **2010**, *4*, 4920–4928.

(3) Espallargas, G. M.; Brammer, L.; Allan, D. R.; Pulham, C. R.; Robertson, N.; Warren, J. E. *J. Am. Chem. Soc.* **2008**, *130*, 9058–9071.

(4) Davis, A. P. *Nature* **2010**, *464*, 169–170.

(5) Alexeev, Y. E.; Kharisov, B. I.; Garcia, T. C. H.; Garnovskii, A. D. *Coord. Chem. Rev.* **2010**, *254*, 794−831.

(6) Miguel, P. J. S.; Amo-Ochoa, P.; Castillo, O.; Houlton, A.; Zamora, E. *Met. Complex-DNA Interact.* **2009**, 95–132.

(7) Cohen, S. M. *Nature* **2009**, *461*, 602–603.

(8) Grimme, S.; Antony, J.; Schwabe, T.; Mueck-Lichtenfeld, C. *Org. Biomol. Chem.* **2007**, *5*, 741–758.

(9) Grimme, S. *Angew. Chem., Int. Ed.* **2008**, *47*, 3430–3434.

(10) Antony, J.; Brueske, B.; Grimme, S. *Phys. Chem. Chem. Phys.* **2009**, *11*, 8440–8447.

(11) Grimme, S. *Chem.—Eur. J.* **2004**, *10*, 3423–3429.

(12) Grimme, S. *J. Comput. Chem.* **2004**, *25*, 1463–1473.

(13) Hyla-Kryspin, I.; Haufe, G.; Grimme, S. *Chem.—Eur. J.* **2004**, *10*, 3411–3422.

(14) Piacenza, M.; Grimme, S. *J. Am. Chem. Soc.* **2005**, *127*, 14841–14848.

(15) Schwabe, T.; Grimme, S. *Phys. Chem. Chem. Phys.* **2006**, *8*, 4398–4401.

(16) Grimme, S.; Mueck-Lichtenfeld, C.; Antony, J. *J. Phys. Chem. C* **2007**, *111*, 11199–11207.

(17) Antony, J.; Grimme, S. *Phys. Chem. Chem. Phys.* **2008**, *10*, 2722–2729.

(18) Grimme, S.; Mueck-Lichtenfeld, C.; Antony, J. *Phys. Chem. Chem. Phys.* **2008**, *10*, 3327–3334.

(19) Pluhackova, K.; Grimme, S.; Hobza, P. *J. Phys. Chem. A* **2008**, *112*, 12469–12474.

(20) Grimme, S. *Org. Lett.* **2010**, *12*, 4670–4673.

(21) Huenerbein, R.; Schirmer, B.; Moellmann, J.; Grimme, S. *Phys. Chem. Chem. Phys.* **2010**, *12*, 6940–6948.

(22) Moriya, M.; Froehlich, R.; Kehr, G.; Erker, G.; Grimme, S. *Chem. Asian J.* **2008**, *3*, 753–758.

(23) Hyla-Kryspin, I.; Grimme, S.; Djukic, J. P. *Organometallics* **2009**, *28*, 1001–1013.

(24) Grimme, S.; Djukic, J.-P. *Inorg. Chem.* **2010**, *49*, 2911–2919.

(25) Schwabe, T.; Grimme, S.; Djukic, J.-P. *J. Am. Chem. Soc.* **2009**, *131*, 14156–14157.

(26) Antony, J.; Grimme, S. *J. Phys. Chem. A* **2007**, *111*, 4862–4868.

(27) Schwabe, T.; Grimme, S. *Phys. Chem. Chem. Phys.* **2007**, *9*, 3397–3406.

(28) Schwabe, T.; Huenerbein, R.; Grimme, S. *Synlett* **2010**, 1431–1441.

(29) Balch, A. L.; Miller, J. J. *Organomet. Chem.* **1971**, *32*, 263–268.

(30) Dart, J. W.; Lloyd, M. K.; McCleverty, J. A.; Mason, R. *J. Chem. Soc. Chem. Commun.* **1971**, 1197–1198.

(31) Branson, P. R.; Green, M. *J. Chem. Soc., Dalton Trans.* **1972**, 1303–1310.

(32) Stejskal, O. E.; Tanner, J. E. *J. Chem. Phys.* **1965**, *42*, 288–292.

(33) Johnson, R. *Prog. Nucl. Magn. Reson. Spectrosc.* **1999**, *34*, 203–256.

(34) Cohen, Y.; Avram, L.; Frish, L. *Angew. Chem., Int. Ed.* **2005**, *44*, 520–554.

2626

dx.doi.org/10.1021/ic102489k |*Inorg. Chem.* 2011, 50, 2619–2628

(35) Lewis, N. S.; Mann, K. R.; Gordon, J. G., II; Gray, H. B. *J. Am. Chem. Soc.* **1976**, *98*, 7461–7463.

(36) Mann, K. R.; Gordon, J. G., II; Gray, H. B. *J. Am. Chem. Soc.* **1975**, *97*, 3553–3555.

(37) Balch, A. L.; Olmstead, M. M. *J. Am. Chem. Soc.* **1976**, *98*, 2354–2356.

(38) Balch, A. L. *J. Am. Chem. Soc.* **1976**, *98*, 8049–8054.

(39) McCleverty, J. A.; Williams, J. *Transition Met. Chem.* **1978**, *3*, 205–211.

(40) Olmstead, M. M.; Balch, A. L. *J. Organomet. Chem.* **1978**, *148*, C15–C18.

(41) Endres, H.; Gottstein, N.; Keller, H. J.; Martin, R.; Rodemer, W.; Steiger, W. *Z. Naturforsch., B: Anorg. Chem., Org. Chem.* **1979**, *34B*, 827–833.

(42) Tran, N. T.; Stork, J. R.; Pham, D.; Olmstead, M. M.; Fettinger, J. C.; Balch, A. L. *Chem. Commun.* **2006**, 1130–1132.

(43) Tran, N. T.; Stork, J. R.; Pham, D.; Chancellor, C. J.; Olmstead, M. M.; Fettinger, J. C.; Balch, A. L. *Inorg. Chem.* **2007**, *46*, 7998–8007.

(44) Miskowski, V. M.; Nobinger, G. L.; Kliger, D. S.; Hammond, G. S.; Lewis, N. S.; Mann, K. R.; Gray, H. B. *J. Am. Chem. Soc.* **1978**, *100*, 485–488.

(45) Miya, S.; Yamamoto, Y.; Yamazaki, H. *Inorg. Chem.* **1982**, *21*, 1486–1488.

(46) Balch, A. L.; Catalano, V. J. *Inorg. Chem.* **1992**, *31*, 3934–3942.

(47) Rice, S. F.; Gray, H. B. *J. Am. Chem. Soc.* **1981**, *103*, 1593–1595.

(48) Miskowski, V. M.; Smith, T. P.; Loehr, T. M.; Gray, H. B. *J. Am. Chem. Soc.* **1985**, *107*, 7925–7934.

(49) Pyykkö, P. *Chem. Rev.* **1997**, *97*, 597–636.

(50) Novoa, J. J.; Aullon, G.; Alemany, P.; Alvarez, S. *J. Am. Chem. Soc.* **1995**, *117*, 7169–7171.

(51) Coppens, P.; Gerlits, O.; Vorontsov, I. I.; Kovalevsky, A. Y.; Chen, Y.-S.; Graber, T.; Gembicky, M.; Novozhilova, I. V. *Chem. Commun.* **2004**, 2144–2145.

(52) Novozhilova, I. V.; Volkov, A. V.; Coppens, P. *Inorg. Chem.* **2004**, *43*, 2299–2307.

(53) Koo, C.-K.; Wong, K.-L.; Lau, K.-C.; Wong, W.-Y.; Lam, M. H.-W. *Chem.—Eur. J.* **2009**, *15*, 7689–7697.

(54) Winkler, J. R.; Marshall, J. L.; Netzel, T. L.; Gray, H. B. *J. Am. Chem. Soc.* **1986**, *108*, 2263–2266.

(55) Stiegman, A. E.; Rice, S. F.; Gray, H. B.; Miskowski, V. M. *Inorg. Chem.* **1987**, *26*, 1112–1116.

(56) Rodman, G. S.; Mann, K. R. *Inorg. Chem.* **1988**, *27*, 3338–3346.

(57) Marshall, J. L.; Hopkins, M. D.; Miskowski, V. M.; Gray, H. B. *Inorg. Chem.* **1992**, *31*, 5034–5040.

(58) Yip, H.; Che, C.; Zhou, Z.; Mak, T. C. W. *J. Chem. Soc., Chem. Commun.* **1992**, 1369–1371.

(59) Ford, P. C.; Vogler, A. *Acc. Chem. Res.* **1993**, *26*, 220–226.

(60) Mealli, C.; Pichierri, F.; Randaccio, L.; Zangrando, E.; Krumm, M.; Holtenrich, D.; Lippert, B. *Inorg. Chem.* **1995**, *34*, 3418–3424.

(61) Kurnikov, I. V.; Zusman, L. D.; Kurnikova, M. G.; Farid, R. S.; Beratan, D. N. *J. Am. Chem. Soc.* **1997**, *119*, 5690–5700.

(62) Fornies-Camer, J.; Masdeu-Bulto, A. M.; Claver, C.; Cardin, C. J. *Inorg. Chem.* **1998**, *37*, 2626–2632.

(63) Lai, S.-W.; Chan, M. C.-W.; Cheung, T.-C.; Peng, S.-M.; Che, C.-M. *Inorg. Chem.* **1999**, *38*, 4046–4055.

(64) Hegmann, T.; Kain, J.; Diele, S.; Schubert, B.; Boegel, H.; Tschierske, C. *J. Mater. Chem.* **2003**, *13*, 991–1003.

(65) Wadas, T. J.; Wang, Q.-M.; Kim, Y.-J.; Flaschenreim, C.; Blanton, T. N.; Eisenberg, R. *J. Am. Chem. Soc.* **2004**, *126*, 16841–16849.

(66) Koo, C.-K.; Lam, B.; Leung, S.-K.; Lam, M. H.-W.; Wong, W.-Y. *J. Am. Chem. Soc.* **2006**, *128*, 16434–16435.

(67) Bercaw, J. E.; Durrell, A. C.; Gray, H. B.; Green, J. C.; Hazari, N.; Labinger, J. A.; Winkler, J. R. *Inorg. Chem.* **2010**, *49*, 1801–1810.

(68) (a) Pyykkö, P.; Li, J.; Runeberg, N. *Chem. Phys. Lett.* **1994**, *218*, 133–138. (b) Pyykkö, P.; Mendizabal, F. *Inorg. Chem.* **1998**, *37*, 3018–3025.

(69) Wu, D.; Chen, A.; Johnson, C. S. *J. Magn. Reson.* **1995**, *A 115*, 260–264.

(70) Tanner, J. E. *J. Chem. Phys.* **1970**, *52*, 2523–2526.

(71) NMRTEC, http://www.nmrtec.com/software/nmrnotebook (Accessed 2011).

(72) Delsuc, M. A.; Malliavin, T. E. *Anal. Chem.* **1998**, *70*, 2146–2148.

(73) Becke, A. D. *Phys. Rev. A* **1988**, *38*, 3098–3100.

(74) Perdew, J. P. *Phys. Rev. B* **1986**, *33*, 8822.

(75) Perdew, J. P. *Phys. Rev. B* **1986**, *34*, 7406.

(76) Perdew, J. P.; Burke, K.; Ernzerhof, M. *Phys. Rev. Lett.* **1996**, *77*, 3865–3868.

(77) Tao, J.; Perdew, J. P.; Staroverov, V. N.; Scuseria, G. E. *Phys. Rev. Lett.* **2003**, *91*, 146401.

(78) Te Velde, G.; Bickelhaupt, F. M.; van Gisbergen, S. J. A.; Fonseca-Guerra, C.; Baerends, E. J.; Snijders, J. G.; Ziegler, T. *J. Comput. Chem.* **2001**, *22*, 931–967.

(79) Baerends, E. J.; Autschbach, J.; Bérces, A.; Bickelhaupt, F. M.; Bo, C.; Boerrigter, P. M.; Cavallo, L.; Chong, D. P.; Deng, L.; Dickson, R. M.; Ellis, D. E.; van Faassen, M.; Fan, L.; Fischer, T. H.; Guerra, C. F.; van Gisbergen, S. J. A.; Götz, A. W.; Groeneveld, J. A.; Gritsenko, O. V.; Grüning, M.; Harris, F. E.; van Hoek, P.; Jacob, C. R.; Jacobsen, H.; Jensen, L.; van Kessel, G.; Kootstra, F.; Krykunov, M. V.; van Lenthe, E.; McCormack, D. A.; Michalak, A.; Neugebauer, J.; Nicu, V. P.; Osinga, V. P.; Patchkovskii, S.; Philipsen, P. H. T.; Post, D.; Pye, C. C.; Ravenek, W.; Rodríguez, J. I.; Ros, P.; Schipper, P. R. T.; Schreckenbach, G.; Snijders, J. G.; Solà, M.; Swart, M.; Swerhone, D.; te Velde, G.; Vernooijs, P.; Versluis, L.; Visscher, L.; Visser, O.; Wang, F.; Wesolowski, T. A.; van Wezenbeek, E. M.; Wiesenekker, G.; Wolff, S. K.; Woo, T. K.; Yakovlev, A. L.; Ziegler, T. In *Amsterdam Density Functional*; ADF2009.01 ed.; SCM, Ed.; Department of Theoretical Chemistry, Vrije Universiteit Amsterdam: The Netherlands, 2009.

(80) Ahlrichs, R. *TURBOMOLE*, version 5.9 ed.; Universität Karlsruhe: Karlsruhe, 2008; http://www.turbomole.com.

(81) Grimme, S. *J. Comput. Chem.* **2006**, *27*, 1787–1799.

(82) Grimme, S.; Antony, J.; Ehrlich, S.; Krieg, H. *J. Chem. Phys.* **2010**, *132*, 154104.

(83) Vosko, S. H.; Wilk, L.; Nusair, M. *Can. J. Phys.* **1980**, *58*, 1200–1211.

(84) van Lenthe, E.; Baerends, E. J.; Snijders, J. G. *J. Chem. Phys.* **1993**, *99*, 4597–4610.

(85) van Lenthe, E.; Ehlers, A. E.; Baerends, E. J. *J. Chem. Phys.* **1999**, *110*, 8943–8953.

(86) van Lenthe, E.; Baerends, E. J. *J. Comput. Chem.* **2003**, *24*, 1142–1156.

(87) Glendening, E. D.; Badenhoop, J. K.; Reed, A. E.; Carpenter, J. E.; Bohmann, J. A.; Morales, C. M.; Weinhold, F. *NBO*, 5.0 ed.; Theoretical Chemistry Institute, University of Wisconsin, Madison, 2001.

(88) Klamt, A.; Schüürmann, G. *J. Chem. Soc.: Perkin Trans. 2* **1993**, 799–805.

(89) Klamt, A. *J. Phys. Chem.* **1995**, *99*, 2224–2235.

(90) Klamt, A.; Jones, V. *J. Chem. Phys.* **1996**, *105*, 9972–9981.

(91) Grimme, S. *J. Chem. Phys.* **2003**, *118*, 9095–9102.

(92) Andrae, D.; Haeussermann, U.; Dolg, M.; Stoll, H.; Preuss, H. *Theor. Chim. Acta* **1990**, *77*, 123–141. For further details see http://www.theochem.uni-stuttgart.de/pseudopotentials/index.en.html.

(93) Weigend, F.; Ahlrichs, R. *Phys. Chem. Chem. Phys.* **2005**, *7*, 3297–3305.

(94) Weigend, F.; Köhn, A.; Hättig, C. *J. Chem. Phys.* **2002**, *116*, 3175–3183.

(95) Eichkorn, K.; Weigend, F.; Treutler, O.; Ahlrichs, R. *Theor. Chem. Acc.* **1997**, *97*, 119–124.

(96) Mann, K. R.; Lewis, N. S.; Williams, R. M.; Gray, H. B.; Gordon, J. G., II *Inorg. Chem.* **1978**, *17*, 828–834.

(97) Exstrom, C. L.; Britton, D.; Mann, K. R.; Hill, M. G.; Miskowski, V. M.; Schaefer, W. P.; Gray, H. B.; Lamanna, W. M. *Inorg. Chem.* **1996**, *35*, 549–550.

(98) Huenerbein, R.; Schirmer, B.; Moellmann, J.; Grimme, S. *Phys. Chem. Chem. Phys.* **2010**, *12*, 6940–6948.

(99) Grimme, S.; Mück-Lichtenfeld, C.; Antony, J. *Phys. Chem. Chem. Phys.* **2008**, *10*, 3327–3334.

(100) Grimme, S. *Angew. Chem., Int. Ed.* **2006**, *45*, 4460–4464.

(101) Magnko, L.; Schweizer, M.; Rauhut, G.; Schütz, M.; Stoll, H.; Werner, H.-J. *Phys. Chem. Chem. Phys.* **2002**, *4*, 1006–1013.

2628

dx.doi.org/10.1021/ic102489k |*Inorg. Chem.* 2011, 50, 2619–2628